UDK 669.14.018.8:621.793:620.193
Original scientific article/Izvirni znanstveni članek

ISSN 1580-2949
MTAEC9, 49(1)19(2015)

CORROSION OF CrN-COATED STAINLESS STEEL IN A NaCl SOLUTION (w = 3 %)

KOROZIJA NERJAVNEGA JEKLA S CrN-PREVLEKO V RAZTOPINI NaCl (w = 3 %)

Israfil Kucuk, Cevat Sarioglu

Marmara University, Dept. of Metallurgical and Materials Engineering, Göztepe kampusu, 34722 Kadiköy-Istanbul, Turkey
cevat.sarioglu@marmara.edu.tr

Prejem rokopisa – received: 2013-09-30; sprejem za objavo – accepted for publication: 2014-02-12

A CrN coating deposited by arc PVD was characterized by XRD and SEM. The in-situ measurement of the corrosion of the CrN-coated substrate was made by corrosion potential (Cor. Pot.), the polarization resistance (PR) method and electrochemical impedance spectroscopy (EIS) in a NaCl solution w = 3 % as a function of the immersion time (about 24 h). A semiconductor scale that formed on the CrN was identified by Mott-Shottky analysis as a p-type semiconductor with flat band potentials, 0.49 V (SCE). The CrN coating (0.5 μm thick) consisted of a mixture of cubic Cr and hexagonal Cr_2N phases exhibiting equiaxed grains and a dense coating with a small quantity of pinholes, voids and porosities. The "transition in corrosion resistance" for the CrN coatings at an early stage was found based on Cor. Pot., PR and EIS data. The CrN did not exhibit any pitting for about 24 h, while the corrosion resistance (R_p and R_{total}) decreased rapidly with time after 5 h of incubation. The transition from high resistance (3 MΩ cm^2) to low resistance (0.24 MΩ cm^2) was explained as a result of the penetration of the electrolyte through the Cr_2O_3 oxide layer to the Cr_2O_3/CrN interface. The resistance of the CrN against pitting corrosion was explained based on the blocking character of the equiaxed, dense, CrN coating against the penetration of the electrolyte.

Keywords: stainless steel, coating, CrN, EIS, polarization resistance, pitting corrosion

CrN-prevleka, nanesena z obločnim PVD-postopkom, je bila pregledana z XRD in SEM. In-situ merjenje korozije podlage s CrN-prevleko je bilo izvršeno z metodo korozijskega potenciala (Cor. Pot.), metodo polarizacijske upornosti (PR) in z elektrokemijsko impedančno spektroskopijo (EIS) v raztopini NaCl (w = 3 %) v odvisnosti od časa namakanja (okrog 24 h). Mott-Shottkyjeva analiza je odkrila nastanek p-vrste polprevodniške plasti s ploščinskim potencialom 0,49 V (SCE). CrN-prevleka (debela 0,5 μm) je sestavljena iz mešanice kubičnega Cr in heksagonalne faze Cr_2N ter ima enakoosna zrna, je gosta, z majhno količino luknjic, praznin in poroznostjo. Na podlagi podatkov Cor. Pot., PR in EIS je bil že v zgodnji fazi ugotovljen "prehod v obstojnost proti koroziji". CrN ni pokazal korozijskih jamic po 24 h, medtem ko se je korozijska upornost (R_p in R_{total}) hitro zmanjšala po 5 h inkubacijskega časa. Prehod iz velike upornosti (3 MΩ cm^2) v majhno (0,24 MΩ cm^2) se razlaga kot rezultat penetracije elektrolita skozi sloj oksida Cr_2O_3 na mejo Cr_2O_3/CrN. Odpornost CrN proti jamičasti koroziji je razložena z zadrževalnim značajem goste, enakoosne prevleke CrN za penetracijo elektrolita.

Ključne besede: nerjavno jeklo, prevleka, CrN, EIS, polarizacijska upornost, jamičasta korozija

1 INTRODUCTION

Hard ceramic coatings such as CrN have mainly been used for tribological applications (e.g., the injection molds for plastic and metals and forming dies).[1–4] CrN coatings possess excellent wear and oxidation resistance and low coefficients of friction. In addition, CrN has been used for decorative applications (particularly for replacing decorative electroplating chrome coatings).[5,6]

Besides the excellent mechanical properties and oxidation resistance, CrN coated on metallic substrates (steel and stainless steels) possesses significant corrosion resistance in saline solutions compared to other hard coatings such as TiN and TiAlN.[7–15] Even though the corrosion resistance of a CrN coating is superior to other coatings, the corrosion resistance of CrN-coated substrates degrades with time.[9,14,15] Generally, this degradation ends up with pitting corrosion by galvanic corrosion between the substrate and the coatings.[14,15] In the literature there has not been sufficient research into degradation and pitting-corrosion mechanisms and the relationships with microstructure.

Martensitic stainless steels (used in this work, EN 1.4034) generally used for blades in kitchen appliances, were coated for both decorative (chrome appearance) and wear-resistance requirements. The corrosion of the CrN coating deposited by arc PVD on a stainless-steel substrate was studied in detail with corrosion potential (Cor. Pot), polarization resistance (PR) and electrochemical impedance spectroscopy (EIS) techniques. The mechanism of corrosion was evaluated with respect to the microstructure of the CrN coating and EIS modelling.

2 EXPERIMENTAL PROCEDURES

The substrate material obtained from ThyssenKrupp was EN 1.4034 (X46Cr13) stainless steel. The composition analysed by optical emission spectroscopy (Q4 Tasman Bruker) was 0.40 C, 0. 44 Si, 0.53 Mn, 14.05 Cr and Fe (balance) (all in mass fractions, w/%). The 4034 stainless steel belonged to the martensitic group of stainless steels and was commercially available annealed and cold-rolled thin-plate form (1.5 mm thickness). The

specimens were cut into widths 50 mm and lengths 100 mm. All the specimens were electropolished for 10 min in a solution containing 30 % H_2SO_4, 60 % H_3PO_4 and 10 % Neutral H_2O at 50 °C with a voltage of 10 V, and then ultrasonically cleaned at 60 °C, dumped in distilled water and dried with nitrogen in order to obtain a clean and smooth corrosion-resistant surface. The electropolished 4034 stainless-steel substrate is subsequently referred to as "substrate" in this paper.

The coating of the substrates was performed in an industrial-sized arc PVD coating chamber (AFS ltd. Cop., Turkey) equipped with six evaporators (cathodes) and rotating substrate holders. During the deposition, four round cathodes (opposing each other) were in use. An Ar glow discharge at a –600 V bias for 10 min was formed in the chamber in order to clean the surface of the substrates. The heating of the substrates was performed with Cr cathodes at about a –800 V bias for about 15 min until the starting temperature reached 350 °C. Then the electropolished specimens were coated with a Cr interlayer for 1 min to improve the adhesion of the coating and later with the CrN layer for 20 min at 1.1×10^{-3} mbar nitrogen pressure and a total pressure of 10^{-2} mbar with a bias voltage of –200 V. The final deposition temperature was 250 °C. The argon gas was purged into the chamber before opening the chamber door.

Electrochemical corrosion units used to perform the EIS, polarization resistance and Mott-Shottky scan were a Gamry PC14/750 Poteniostat/Galvanostat/ZRA System equipped with DC105 corrosion testing and an EIS300 A/C (10 mHz to 300 kHz). All the tests were performed in a NaCl 0.5 M (w = 3 %) aerated water solution at 25 °C using a three-electrode system (working (sample), auxiliary (graphite) and reference (standard calomel electrode (SCE)) using a Gamry paint cell unit. This Gamry Paint cell unit, presented in **Figure 1** and used for flat plate samples, consisted of a hollow glass cylinder (capacity 50 mL) mounted on a plate sample using a stainless-steel clamp with an O-ring. The exposed surface area of all the samples was kept at 15 cm^2, the maximum value without using a mask in order to incorporate a statistically significant number of defects in the CrN coatings. The computer-controlled automatic measurements (corrosion potential, polarization resistance and EIS) were carried out in the following order: 10 min cor. pot; 2.7 min PR; 5 min waiting period; and 8 min EIS meas. for each cycle 68 min during a total of about 24 h of exposure after the corrosion potential was stable. The amplitude of the AC voltage was selected to be 10 mV with respect to the corrosion potential in the EIS. During the polarization resistance scan the corrosion potential was changed by 20 mV with a 0.25 mV/s scan rate from the cathodic to the anodic polarization directions. Mott-Shottky analyses at a frequency of 1 Hz between +430 mV and –570 mV were performed on a CrN-coated substrate after the corrosion potential was stable.

A microstructural analysis of the uncoated and coated samples was performed before and after the corrosion using a scanning electron microscope (SEM, Jeol, JSM-5910LV) and energy-dispersive spectroscopy (EDS). The cross-section of the coatings was observed after fracture in liquid nitrogen. X-ray diffraction (Rigaku, D-MAX 2200, Cu K_α radiation) was used to identify the structure of the coatings deposited on the substrate.

3 RESULTS

3.1 Microstructural characterization of CrN coated substrate

The 4034 EP stainless-steel substrate possessed a ferritic structure (α-Fe) matrix (**Figure 2**) with a homogenous distribution of the carbide phases (Cr and C-rich phase identified by EDS). After coating with CrN at 1.1×10^{-3} mbar of N_2 partial pressure, the surface morphology of the CrN coatings reflected the morphology of

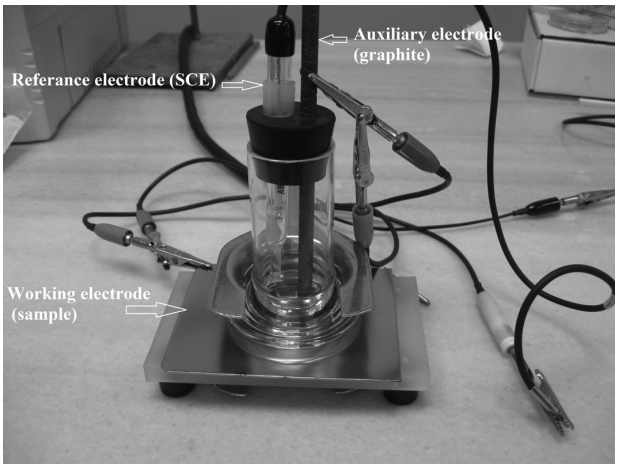

Figure 1: Gamry paint cell used in this work for electrochemical measurements

Slika 1: Elektrokemijske meritve so bile izvršene z Gamryjevo celico za preizkušanje barvnih premazov

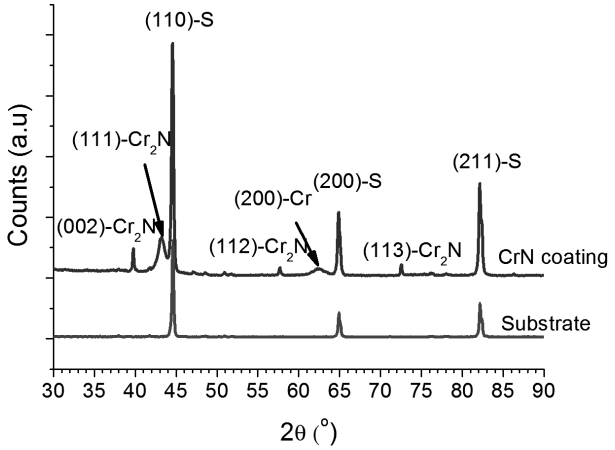

Figure 2: 2θ scan obtained from EP 4034 steel substrate and CrN-coated substrates using Bragg-Brentano symmetric X-ray diffraction

Slika 2: Posnetek 2θ z Bragg-Brentanovo simetrično rentgensko difrakcijo podlage iz jekla EP 4034 in iz podlage s prevleko CrN

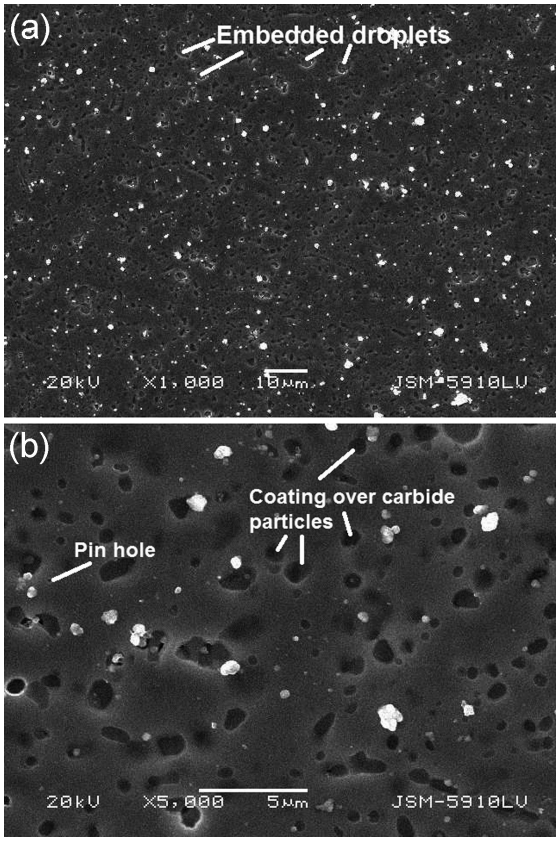

Figure 3: SEM (SEI) micrographs taken from the CrN coating surface at: a) low magnification and b) high magnification. The CrN coating deposited on the carbide phases was distinguished with a depression over the surface at a) and b) and was marked at b). Embedded droplets were marked at a). Bright particles on coating surface at a) and b) were un-embedded droplets (spherical particles).

Slika 3: SEM (SEI)-posnetka površine prevleke CrN pri: a) majhni povečavi in b) veliki povečavi. CrN-prevleke na karbidnih fazah so ločene s poglobitvijo na površini a) in b) in označene na b). Vgnezdene kapljice so označene na a). Svetli delci na površini prevleke a) in b) so nevgnezdene kapljice (sferični delci).

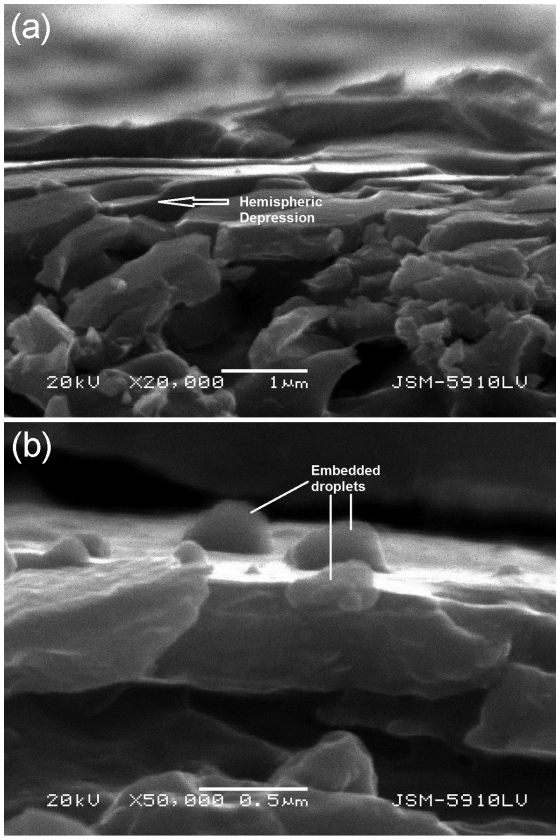

Figure 4: SEM (SEI) micrographs of fractured surface (in liquid nitrogen) of CrN coating from different areas a) and b). Equiaxed grains through the fractured coating were seen at high magnification b). Embedded particles were marked at b). Hemispheric depression in fractured coating was shown at a).

Slika 4: SEM (SEI)-posnetka površine preloma (v tekočem dušiku) CrN-prevleke z različnih področij a) in b). Pri veliki povečavi so vidna enakoosna zrna na prelomu prevleke. Vgnezdeni delci so označeni na b). Polkrožna poglobitev na prelomu prevleke je prikazana na a).

the EP substrate surface where etched carbide phases were covered by the CrN coating (**Figure 3**). The same observations were made for the cross-section micrographs of the CrN-coated substrates where the coatings formed on the carbide phases represented a hemispheric depression (**Figure 4**). Based on a detailed surface and cross-section investigation, it was found that the CrN coatings (**Figures 3** and **4**) exhibited a dense coating morphology (a small quantity of pinholes and porosities) with equiaxed grains (less than 100 nm grain size) and smooth coverage over the carbide precipitates and matrix. The thickness of the CrN coatings measured from the cross-section (**Figure 4**) was about 0.5 μm.

Due to the arc PVD process, droplets formed on the surface of the CrN-coated substrate. There were two different types of droplets found on the surface of the CrN coatings, the droplets embedded in the scale, the coating and the un-embedded macro-particles (spherical bright particles) (**Figures 3** and **4**). They were believed to deposit on the surface as a result of vapour-phase precipitation after the coating was finished (when a bias was interrupted). Both types of droplets analysed by EDS contained mainly Cr and N (Cr-rich particles). The CrN coating contained cubic Cr and hexagonal Cr_2N phases. The Cr peak exhibited line broadening and a shift in the line position of the (200) peak due to the dissolution of nitrogen in the Cr and a small crystallite size (**Figure 2**).

3.2 In-situ measurement of the corrosion of the CrN-coated substrate during 24 h of exposure with corrosion potentials, PR- and EIS-measurements

The corrosion potentials were plotted as a function of exposure time in **Figure 5**. The corrosion potential of the substrate (–468 mV (SCE) at 20 min) dropped rapidly and reached a steady-state value of –620 mV (SCE) within 180 min (3 h) (**Figure 5**). The corrosion potential of the CrN remained at around –150 mV (SCE) up to 267 min before decreasing to a level close to the substrate's potential value (**Figure 5**). At all times the corrosion potential of the substrate was lower compared to the

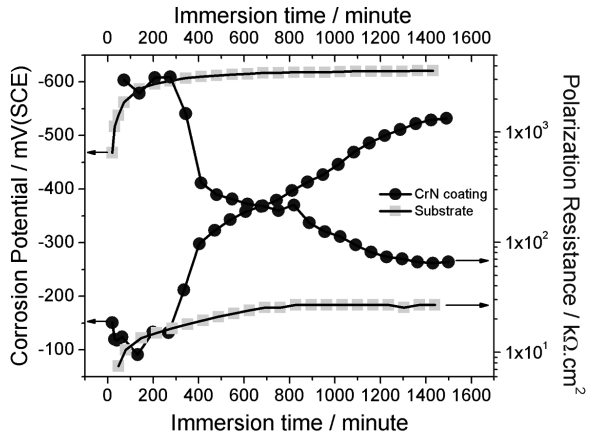

Figure 5: Corrosion potentials and polarization resistance (R_p) of the substrate and CrN-coated substrates determined from polarization resistance scan in NaCl (w = 3 %) solution as a function of immersion time

Slika 5: Korozijski potenciali in polarizacijska upornost (R_p) podlage in CrN-prevleke, določeni s posnetka polarizacijske upornosti v raztopini NaCl (w = 3 %) v odvisnosti od časa namakanja

CrN coating during about 24 h of exposure. The surface appearance of the uncoated substrate and the CrN-coated substrate did not vary during the 24 h of exposure.

The polarization-resistance values (R_p) were determined using the polarization resistance method and plotted (**Figure 5**). The polarization resistance (R_p) of the CrN coatings (**Figure 5**), deduced from the plots in **Figure 6**, remained at a high level of 3 MΩ cm² until 267 min and then rapidly decreased from 3 MΩ cm² to 0.24 MΩ cm² within the next 272 min. This decrease could be detected in the polarization plots (expansion of the x-axis) (**Figure 6**). After 1491 min the polarization resistance decreased to 66 kΩ cm². The plateau in the polarization resistance up to 267 min matched with the plateau in the corrosion potentials in the same exposure range (**Figure 5**). The polarization resistance (R_p) of the substrate increased up to 27 kΩ cm² with time (**Figure 5**).

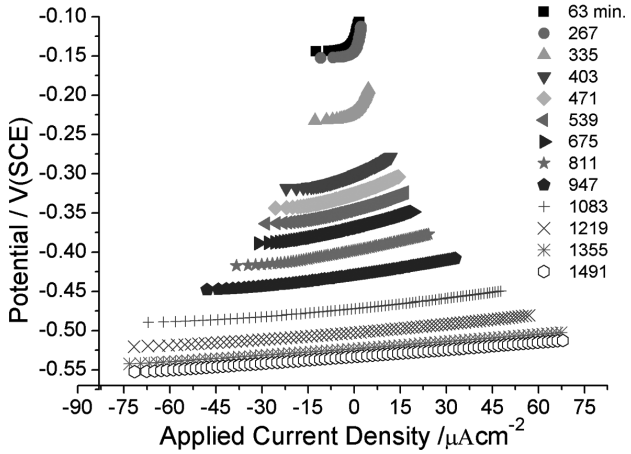

Figure 6: Polarization resistance scan of CrN coating in NaCl (w = 3 %) solution as a function of immersion time

Slika 6: Posnetek polarizacijske upornosti CrN-prevleke v raztopini NaCl (w = 3 %) v odvisnosti od časa namakanja

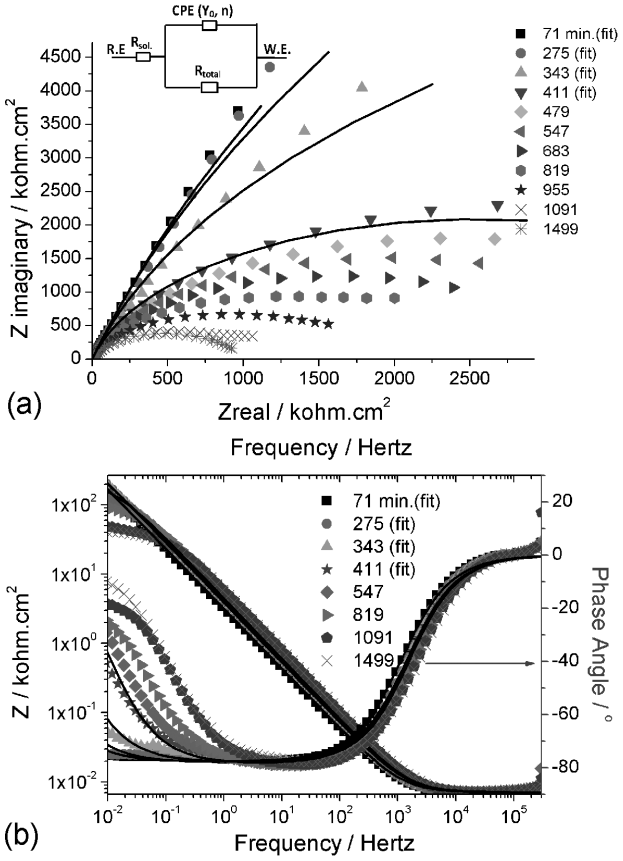

Figure 7: EIS data of CrN coating for selected immersion time: a) Nyquist plots and b) the Bode plots

Slika 7: EIS-podatki za CrN-prevleko pri izbranih časih namakanja: a) Nyquistov diagram in b) Bodejev diagram

After about 24 h the R_p of the CrN coating was two times greater than the R_p of the substrate (**Figure 5**).

The Bode and Nyquist plots of the CrN coatings from the EIS measurements are shown in **Figure 7**. At the beginning of the immersion in the salt solution, the Bode and Nyquist plots exhibited a strong capacitive behaviour. In the Bode plot (**Figure 7b**), the plateau in the phase shift (at about –80°) extended to the whole low-frequency region and the almost perpendicular line in the Nyquist plot indicated a strong imaginary part of the impedance (a strong capacitive character) (**Figure 7a**). Between 275 min and 411 min, the Bode and Nyquist plots changed noticeably, the plateau in the low-frequency region shrank and the Nyquist plot's shape changed from a line to an arch (**Figure 7a**). The evolution of the impedance spectrum coincided with the change in the corrosion potential (**Figure 5**) and the polarization resistance during the first 411 min of exposure in the salt solution (**Figures 5** and **6**). The one time constant clearly appeared in the Bode plot (**Figure 7b**). The imaginary impedance values decreased, resulting in the shrinkage of the arch in the Nyquist plot (**Figure 7a**). During 24 h of exposure to the salt solution there were no pits and no colour changes on the surface

of the CrN coatings, while the impedance values continued to decrease (**Figure 7**).

3.3 The Mott-Shottky measurements

The Mott-Shottky measurements were made for the CrN coating and plotted in **Figure 8**. Before the Mott-Shottky measurement was made the corrosion potential was stable and the EIS data indicated a strong capacitive response at an early stage of the exposure (after 60 min). The plot for CrN (**Figure 8**) showed a linear part with a negative slope between 110 mV and 435 mV (SCE). The negative slope implied that there was a p-type semiconductor oxide layer on the CrN surface.

4 DISCUSSION

4.1 Structure of CrN coating

The CrN coating exhibited a mixture of two phases of Cr and Cr_2N in the N_2 partial pressure of 1.1×10^{-3} mbar (**Figure 2**). Significant peak broadening of the (200) plane and a shift in the peak position were observed for Cr. Similar results were found by Barata.[16] With increasing nitrogen content, Cr, Cr_2N, CrN and mixtures of these phases were obtained, based on reports in[16–21]. The Cr phase was soft, while the Cr_2N phase was hard.[16,18,22] The CrN coatings in this work exhibited significant ductility, as can be seen from the fractured cross-section (**Figure 4**). Droplets, considered as a preferential site for pitting in[8], were found on the CrN coating (**Figures 3** and **4**). The CrN coating exhibited a very dense and very smooth surface over the substrate, including etched carbide phases and droplets, resulting in less porosity and fewer pinholes. Thus, the CrN coating could effectively prevent the electrolyte from reaching the CrN coating/substrate interface directly.

The development of an equiaxed grain morphology (**Figure 4**) requires significant mobility of the adatoms during the growth of the coating according to the structure zone model (SZM).[8] The equiaxed grain morphology was observed for similar coating conditions in[6,14,15]. In addition, from the surface and cross-section micrographs (**Figures 3** and **4**) it was clear that the CrN coating was dense and provided smooth coverage over the etched carbide phases, indicating significant surface mobility of the adatoms. In the structure Zone Model, the T_S/T_M ratio, where T_S is the substrate deposition temperature (taken as an average of 300 °C) and T_M is the melting temperature of the coating, determines the morphology of coatings (equiaxed vs. columnar) together with the bias voltage and the total pressure.[3] As the ratio increases the coating morphology becomes more equiaxed due to an increase in the surface mobility.[3] When the melting point of the CrN coatings is taken as T_M (Cr) = 1907 °C [23] and T_M (Cr_2N) = 1500 °C [24], the ratio of T_S/T_M for CrN is in the range 0.26–0.32. For this ratio range we expected to observe significant surface mobility for the CrN coatings according to SZM[3], supporting the observation of equiaxed grains, and the denser and smoother coverage of the CrN coating.

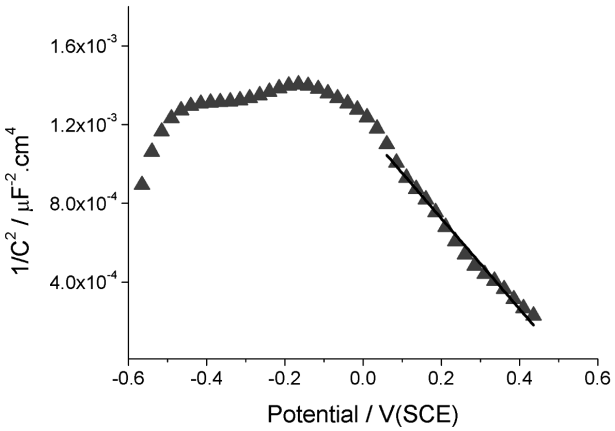

Figure 8: The Mott-Shottky measurements made for CrN coatings at frequency of 1 Hz in NaCl (w = 3 %) solution

Slika 8: Mott-Shottkyjeva meritev CrN-prevleke pri frekvenci 1 Hz v raztopini NaCl (w = 3 %)

4.2 Mott-Shottky analysis of CrN coatings

In the literature, the Mott-Shottky analysis has been used to characterize the semiconductor layer formed on the surface of the materials and coatings.[9,25–30] Based on **Figure 8**, it was concluded that the semiconductor layer formed on the CrN-coated substrate was p-type (presumably Cr_2O_3). In agreement with this result, Lavigne[31] and Mendibide[9] found p-type Cr_2O_3 on the CrN coating deposited by PVD on glass substrates.

The Mott-Shottky equation on page 127 in[25] was used to determine the flat band potential and the density of the charge (the density of acceptors for the p-type semiconductor) in the space-charge region. After taking the dielectric constant of the Cr_2O_3 as 30 (cited in[26] as ref. 17), the flat band potentials and the density of charges were determined from the linear portion of the plot in **Figure 8** using the equation in[25]. The density of acceptors in the space-charge region in the p-type Cr_2O_3 was 2.14×10^{25} cm^{-3}. Lavigne[31] obtained a density of the acceptors of 1.3×10^{20} cm^{-3} for the p-type oxide scale (mainly Cr_2O_3) formed on the CrN coating in a solution of Na_2SO_4 0.07 M and a small addition of H_2SO_4 with pH = 4. The Cr_2O_3 scales with the high charge densities ($10^{20–25}$ cm^{-3}) in the space-charge layer were considered as highly doped semiconductor layers.[25] The flat bond potentials indicated the position of the valance-band edge for the p-type Cr_2O_3 since the Fermi levels were generally close to the valance-band edge for the p-type.[25] The calculated flat band potentials from the intercept of the plots (**Figure 8**) was +0.49 V (SCE) for the p-type Cr_2O_3. The flat band potential reported for the oxide scale for a similar coating and nitrogen pressure by Lavigne[31] was in agreement with this result after considering the pH effect.

4.3 Corrosion of CrN-coated substrate and EIS modelling

Even though there was no colour change or pitting on the CrN-coated substrate during immersion, the transition in PR and EIS data (this transition was reproduced) from more resistance to less resistance at the early stage between 275 min and 411 min was found simultaneously using the EIS and PR measurements (**Figures 5** and **7**). The EIS data was modelled as a one-time constant (**Figure 7a**), the same as the EIS model for the substrate since there was no pitting corrosion and the EIS data exhibited one time constant (**Figure 7**). The total polarization resistance ($R_{total} = R_{passive} + R_{pore}$) included the resistance of the passive layer ($R_{passive}$) and the pore resistance (R_{pore}) to where the electrolyte gained access. The fitted EIS data are presented in **Figure 7** and **Table 1**. The $\chi 2$ values were in the range of $2–10 \times 10^{-3}$, while the n value was about 0.88 and remained constant with time. The polarization resistance (R_p) and the total resistance (R_{total}) determined from the EIS data were almost the same (**Figure 9**). The R_{total} values dropped rapidly from about 2.62 MΩ cm^2 levels to 0.33 MΩ cm^2 levels between 275 min and 411 min (in about 2 h) (**Figure 9**). In the same time interval, the admittance, Y_0 (**Figure 10** and **Table 1**), decreased from 34.6 μcm^{-2} s^n Ω to 29.7 μcm^{-2} s^n Ω by 14 %, indicating an increase in the capacitive behaviour of the passive layer (Cr_2O_3). The total resistance of the capacitive layer R_{total} and R_p continued to decrease gradually after 411 min until the end of the exposure (1499 min) to the level of 60 kΩ cm^2 without any observation of pitting on the CrN surface (**Figures 5** and **9**). The corrosion potential also followed the same trend with the EIS and PR results (**Figures 5** and **9**).

Table 1: The EIS fit parameters of the CrN coating from the electrical circuit model (EC model); Y_0, n, $R_{sol.}$ and R_{total} were determined by the best non-linear least-square fit with a goodness of the fit value ($\chi 2$)

Tabela 1: EIS-parametri CrN-prevleke iz modela električnega tokokroga (EC-model); Y_0, n, $R_{sol.}$ in R_{total} so bili določeni z najboljšim ujemanjem nelinearnih najmanjših kvadratov z vrednostjo ujemanja ($\chi 2$)

Immersion time (min)	R_{sol}/ (Ω cm^2)	R_{total}/ (kΩ cm^2)	Y_0/ (μcm^{-2} s^n Ω)	n	Goodness of Fit ($\chi 2 \times 10^{+3}$)
71	10.6	3457.5	42.8	0.86	2.143
275	10.6	2632.5	34.6	0.87	4.065
343	10.6	1054.5	33.1	0.87	4.014
411	10.6	340.5	29.7	0.88	3.299
819	10.7	195	24.6	0.88	2.72
1091	10.7	109.5	22.7	0.88	10.18
1499	10.6	63	23	0.88	2.237

It was believed that a rapid drop in the corrosion potential and the polarization resistance (R_p and R_{total}) of the passive oxide (Cr_2O_3) between 275 min and 411 min (in the transition period) (**Figure 9**) was due to penetration of the electrolyte into the CrN coating/Cr_2O_3 interface. Once the electrolyte reached this interface, the galvanic coupling between the passive layer (Cr_2O_3) and the bare mixture of the Cr and Cr_2N surfaces (CrN surface) proceeded and polarization on both areas (the cathodic polarization on the Cr_2O_3 scale, the anodic polarization on the bare CrN coatings) took place. The new corrosion potential established (more cathodic, more negative) as observed (**Figures 5** and **9**).

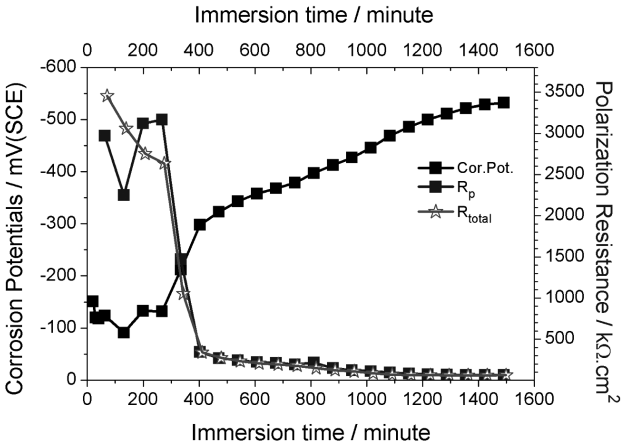

Figure 9: Corrosion potential (Cor. Pot.), polarization resistance (R_p and R_{total} calculated from EIS data) for the CrN coating in NaCl (w = 3 %) solution as a function of immersion time

Slika 9: Korozijski potencial (Cor. Pot.), polarizacijska upornost (R_p in R_{total}, izračunani iz podatkov EIS) CrN-prevleke v raztopini NaCl (w = 3 %) v odvisnosti od časa namakanja

After 411 min, the polarization resistance (R_p and R_{total}) and the corrosion potential continued to drop gradually (**Figures 5** and **9**). This could be explained as follows. The anodic areas of the bare exposed surface in the CrN scale increased with the penetration of the electrolyte into the Cr_2O_3/CrN interface and towards the substrate/CrN coating interface through equiaxed grain boundaries, pinholes and embedded droplets. The increase in the anodic areas increased the anodic currents

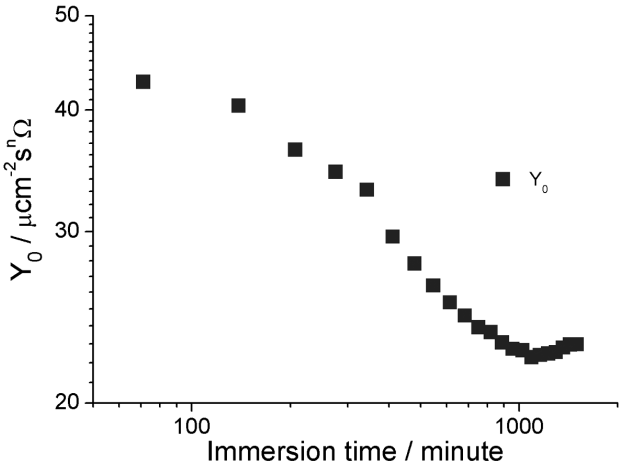

Figure 10: Admittance (Y_0) for the CrN coating in NaCl (w = 3 %) solution as a function of immersion time

Slika 10: Admitanca (Y_0) za CrN prevleko v raztopini NaCl (w = 3 %) v odvisnosti od časa namakanja

and cathodic currents, resulting in a more cathodic polarization of the Cr_2O_3 surface as bare surfaces of CrN coating continued to be exposed to the electrolyte with the immersion time. As a result of this, the polarization resistance and corrosion potentials decreased, as was observed (**Figures 5** and **9**).

In aerated salt solution (w(NaCl) = 3 %) with pH = 8 and at the corrosion potential range (**Figure 5**), the Pourbaix diagram for the Cr indicated that the Cr could exhibit passivation and the anodic polarization of surface could result in passivation.[32] Mixture phases (Cr and Cr_2N) of the CrN coating were thought to behave in a similar way to the pure Cr phase when the surface was anodically polarized in the saline solution. In support of this, Lavigne[31] observed a passive layer on the Cr and Cr + Cr_2N coating in a pH = 4 solution. Passivation could continue with time until the substrate containing Fe is reached. The electrolyte was believed to not yet reach the substrate/CrN interface since no pit or Fe oxide residue (brownish colour residue) on the surface after 24 h was observed.

The Y_0 (measure of capacity) value decreased with time logarithmically up to 1091 min (**Figure 10**). The capacity (C) decreases either with a decrease in the dielectric constant of the Cr_2O_3 passive film and the area of the passive film or an increase in the thickness of the Cr_2O_3 oxide layer. Both the area of the passive layer could increase (as explained above) and the passive film of Cr_2O_3 on Cr or Cr_2N coating could grow in this solution of pH = 8 during immersion in a 3 NaCl (w = 3 %) solution.

The corrosion resistance of the CrN was greater than the substrate during about 24 h of exposure (**Figure 5**), indicating more resistance to the passive scale on the CrN-coated substrate in the NaCl (w = 3 %) solution. Also, the corrosion resistance of the CrN coating was more resistance than that of the TiN coating under similar deposition conditions.[33] Similar results were reported in the literature for different PVD processes and coating conditions.[8–15] There were two main differences in the microstructural morphologies between the TiN and CrN coatings for the same deposition condition.[14,15,33] First, the CrN exhibited equiaxed grains (**Figure 4**), while the TiN coating was columnar. Second, the CrN coating was denser (contained a smaller quantity of pinholes and fewer porosities) compared to the TiN coating. The CrN coatings with equiaxed grains were believed to suppress the time for the electrolyte to reach the substrate interface by increasing the diffusion length (more grain boundaries) (**Figure 4**).[14,15] In addition to this, with denser and better coverage of the CrN coatings over the substrate, it resisted more against the penetration of the electrolyte, delaying the pitting corrosion (**Figures 3** and **4**). On the other hand, the TiN coating with columnar grain boundaries extending from the surface to the substrate interface and containing more porosity (pinholes, voids, cracks and less coverage) allowed the electrolyte to reach the interface easily. As a result of this, the pitting formation and growth as captured by the PR and EIS measurements took place on the TiN coating as quickly as after 1 h. In conclusion, the blocking character of the coating against the penetration of the electrolyte driven by galvanic corrosion was found to be the predominant factor in the corrosion of CrN and TiN.

5 CONCLUSIONS

1. The corrosion of CrN is directly related to the coating defects and coating structure. The CrN coating deposited on the substrate consisted of a mixture of cubic Cr and hexagonal Cr_2N and a passive p-type oxide (presumably Cr_2O_3) film, determined by Mott-Shottky analysis. The CrN coating consisted of equiaxed grains and a smooth coverage over the substrate surface, resulting in a dense coating morphology with a small quantity of pin holes and porosities.
2. The CrN did not exhibit any pitting for about 24 h, while the corrosion resistance (R_p and R_{total}) decreased rapidly with time after 5 h of incubation time. Based on the PR and EIS results, the transition from high resistance (3 MΩ cm^2) to low resistance (0.24 MΩ cm^2) was explained as a result of the penetration of the electrolyte through the Cr_2O_3 oxide layer to the Cr_2O_3/CrN interface.
3. The corrosion resistance (R_p and R_{total}) of CrN was greater than that of the TiN and the substrate during about 24 h of immersion in NaCl (w = 3 %) solution. The cause of the greater corrosion resistance of the CrN was explained on the basis of the greater blocking character of the equiaxed, dense, CrN coating against the penetration of the electrolyte through the coatings compared to the columnar, porous, TiN coating.

Acknowledgement

Marmara University is greatly acknowledged for financial support through the Contract (No: FEN-KPS-080808-0178).

6 REFERENCES

[1] B. Warchholinski, A. Gilewicz, Surface Engineering, 27 (**2011**) 7, 491–497

[2] E. Lugscheider, K. Bobzin, Th. Horning, M. Macs, Thin Solid Films, 420–421 (**2002**), 318–323

[3] C. Ducros, V. Benevent, F. Sanchette, Surface and Coatings Technology, 163–164 (**2003**), 681–688

[4] L. Hultman, J. E. Sundgren, Structure/property relationships for hard coatings, In: R. F. Bunshah (ed.), Handbook of Hard Coatings, William Andrew Publishing, New York 2001, 108–180

[5] B. Navinsek, P. Panjan, I. Milosev, Surf. Cot. Tech., 116–119 (**1999**), 476–487

[6] A. Hurkmans, D. B. Lewis, W. D. Munz, Surface Engineering, 19 (**2003**) 3, 205–210

[7] H. A. Jehn, Surface and Coatings Technology, 125 (**2000**), 212–217

[8] M. Fenker, M. Balzer, H. Kappl, Thin Solid Films, 515 (**2006**) 1, 27–32
[9] C. Mendibide, P. Steyer, J. P. Millet, Surface and Coatings Technology, 200 (**2005**), 109–112
[10] M. Urgen, A. F. Cakir, Surface and Coatings Technology, 96 (**1997**), 236–244
[11] M. A. M. Ibrahim, S. F. Korablov, M. Yoshimura, Corrosion Science, 44 (**2002**), 815–828
[12] V. K. William Grips, H. C. Barshilia, V. Ezhil Selvi, Kalavati, K. S. Rajam, Thin Solid Films, 514 (**2006**), 204–211
[13] L. Cunha, M. Andritschky, L. Rebouta, R. Silva, Thin Solid Films, 317 (**1998**), 351–355
[14] C. Liu, Q. Bi, A. Leyland, A. Matthews, Corrosion Science, 45 (**2003**), 1243–1256
[15] C. Liu, Q. Bi, A. Leyland, A. Matthews, Corrosion Science, 45 (**2003**), 1257–1273
[16] A. Barata, L. Cunha, C. Moura, Thin Solid Films, 398–399 (**2001**), 501–506
[17] E. Forniés, R. Escobar Galindo, O. Sánchez, J. M. Albella, Surface and Coatings Technology, 200 (**2006**), 6047–6053
[18] S. K. Pradhan, C. Nouveau, T. A. Vasin, M. A. Djouadi, Surface and Coatings Technology, 200 (**2005**), 141–145
[19] Z. B. Zhaoa, Z. U. Rekb, S. M. Yalisovec, J. C. Bilell, Surface and Coatings Technology, 185 (**2004**), 329–339
[20] B. C. Ruden, E. Restrepo-Parra, A. U. Paladines, F. Sequeda, Applied Surface Science, 270 (**2013**), 150–156
[21] P. Hones, R. Sanjines, F. Levy, Surface and Coatings Technology, 91–95 (**1997**), 398–402
[22] P. Engel, G. Schwarz, G. K. Wolf, Surface and Coatings Technology, 98 (**1998**), 1002–1007
[23] R. T. DeHoff, Thermodynamics in materials science, McGraw-Hill, Inc., 1993
[24] W. Kim, C. Y. Suh, K. M. Roh, J. W. Lim, S. L. Du, I. J. Shan, Materials Transactions, 53 (**2012**) 8, 1543–1546
[25] S. Roy Morrison, Electrochemistry at Semiconductor and Oxidized Metal Electrodes, Plenum Press, New York 1980
[26] S. Rudenja, C. Leygraf, J. Pan, P. Kulu, E. Talimets, V. Mikli, Surface and Coatings Technology, 114 (**1999**), 129–136
[27] J. Wielant, V. Goossens, R. Hausbrand, H. Terryn, Electrochimca Acta, 52 (**2007**), 7617–7625
[28] K. S. Raja, D. A. Jones, Corrosion Science, 48 (**2006**), 1623–1638
[29] N. E. Hakiki, M. F. Montemor, M. G. S. Ferreira, M. da Cunha Belo, Corrosion Science, 42 (**2000**), 687–702
[30] G. Goodlet, S. Faty, S. Cardoso, P. P. Freitas, A. M. P. Simoes, M. G. S. Ferreira, M. Da Cunha Belo, Corrosion Science, 46 (**2004**), 1479–1499
[31] O. Lavigne, C. Alemany-Dumont, B. Normand, M. H. Berger, C. Duhamel, P. Dekichere, Corrosion Science, 53 (**2011**), 2087–2096
[32] D. A. Jones, Principles and Prevention of Corrosion, Prentice hall, Inc., 1992
[33] I. Kucuk, Corrosion of hard ceramic (TiN, CrN) coatings deposited on stainless steels, Master Thesis, Sakarya University, Turkey, 2009